

Supporting Information

Preparation of porous carbon electrodes from semen cassiae for high-performance electric double-layer capacitors

Ji-Shi Wei,^a Suige Wan,^b Peng Zhang,^a Hui Ding,^c Xiao-Bo Chen,^d Huan-Ming Xiong*,^a Shuyan Gao,^b Xianjun Wei*^b

^a Department of Chemistry and Shanghai Key Laboratory of Molecular Catalysis and Innovative Materials, Fudan University, Shanghai 200433, P. R. China.

^b Key Laboratory of Green Chemical Media and Reactions (Ministry of Education) and School of Chemistry and Chemical Engineering, Henan Normal University, Xinxiang Henan 453007, P. R. China

^c College of Chemical Engineering, China University of Mining and Technology, Xuzhou Jiangsu 221008, P. R. China

^d School of Engineering, RMIT University, Carlton, VIC 3053, Australia

*Corresponding Authors: E-mail: hmxiong@fudan.edu.cn; xj_wei@163.com.

This file includes:

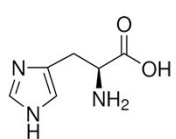
Fig. S1 to S11

Tables S1 to S3

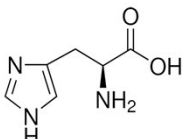
References S1-S11

Figures and Tables

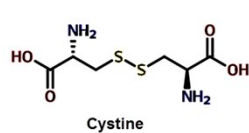
Amino acids



Aspartic acid

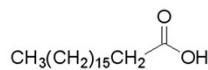


Histidine

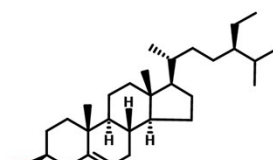


Cystine

Fatty Acids



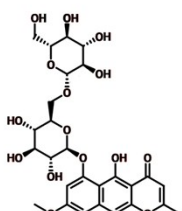
stearic acid



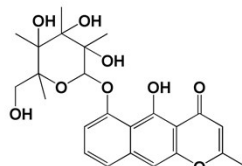
Stigmasterol; (24S)-24-Ethylcholesta-5,22-dien-3 β -ol

Unsaponifiable matters

Naphthopyrone

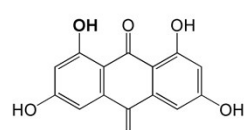


Rubrofusarin-6- β -gentioside; 4H-Naphtho[2,3-b]pyran-4-one,6-[(6-O- β -D-glucopyranosyl- β -D-glucopyranosyloxy]-5-hydroxy-8-methoxy-2-methyl-

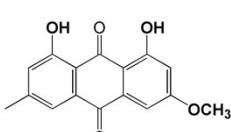


Cassiaside; 5-hydroxy-2-methyl-6-[(2S,3R,4S,5S,6R)-3,4,5-trihydroxy-6-(hydroxymethyl)oxan-2-yl]oxybenzo[*g*]chromen-4-one

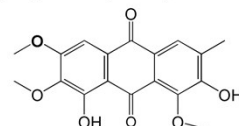
Anthraquinone



Emodin; 1,3,8-Trihydroxy-6-methylantraquinone



Phycion; 1,8-dihydroxy-3-methoxy-6-methylantracene-9,10-dione



Obtusin; 1,7-Dihydroxy-2,3,8-trimethoxy-6-methylantracene-9,10-dione

Fig. S1 molecular formulas of main components in semen cassia. Semen cassia with complex components, which include amino acids, fatty acids, naphthopyrone and so on. And molecular formulas of these main components are listed above.

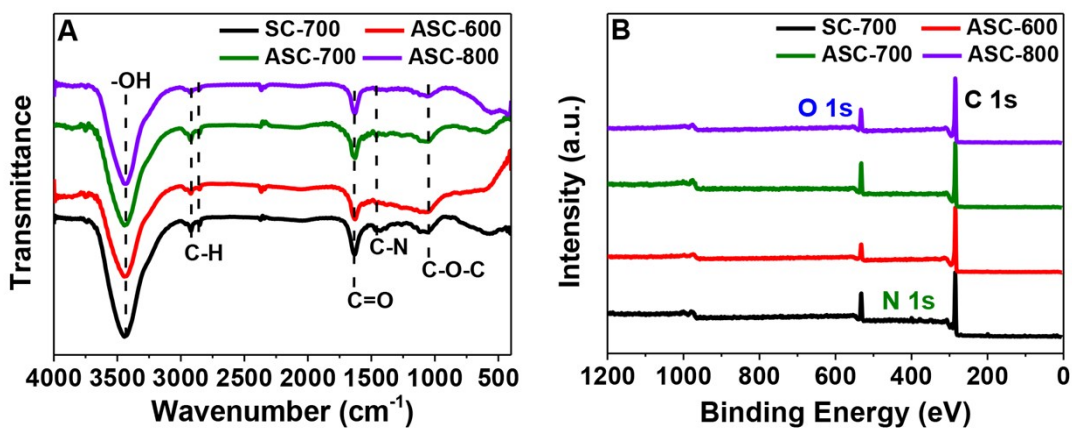


Fig. S2 (A) FTIR spectra and (B) XPS survey spectra.

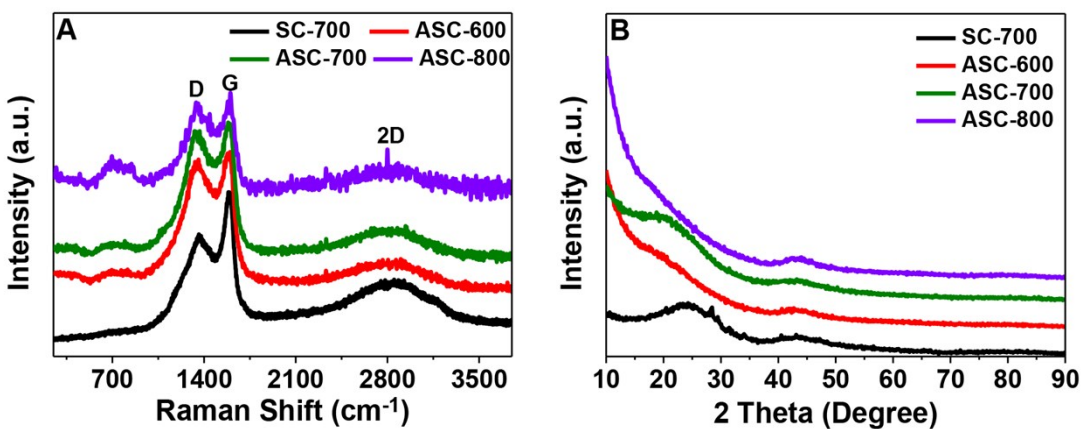


Fig. S3 (A) Raman spectra and XRD patterns.

Table S1 Surface atomic percentage of nitrogen and oxygen derived from XPS results

| Samples | Species concentration (at.%) | | | N 1s at.% | | | O 1s at.% | | |
|---------|------------------------------|------|-------|-----------|------|------|-----------|------------|------|
| | C1s | N1s | O1s | N-6 | N-5 | N-X | C=O | C-O-C/C-OH | COOH |
| SC-700 | 81.93 | 2.43 | 15.64 | 1.06 | 0.82 | 0.55 | 5.30 | 4.98 | 5.36 |
| ASC-600 | 86.79 | 0.92 | 16.12 | 0.50 | 0.42 | - | 5.78 | 4.83 | 5.51 |
| ASC-700 | 88.63 | 0.46 | 10.91 | 0.25 | 0.21 | - | 3.42 | 3.16 | 3.33 |
| ASC-800 | 87.94 | 0 | 12.06 | - | - | - | 4.17 | 3.88 | 4.01 |

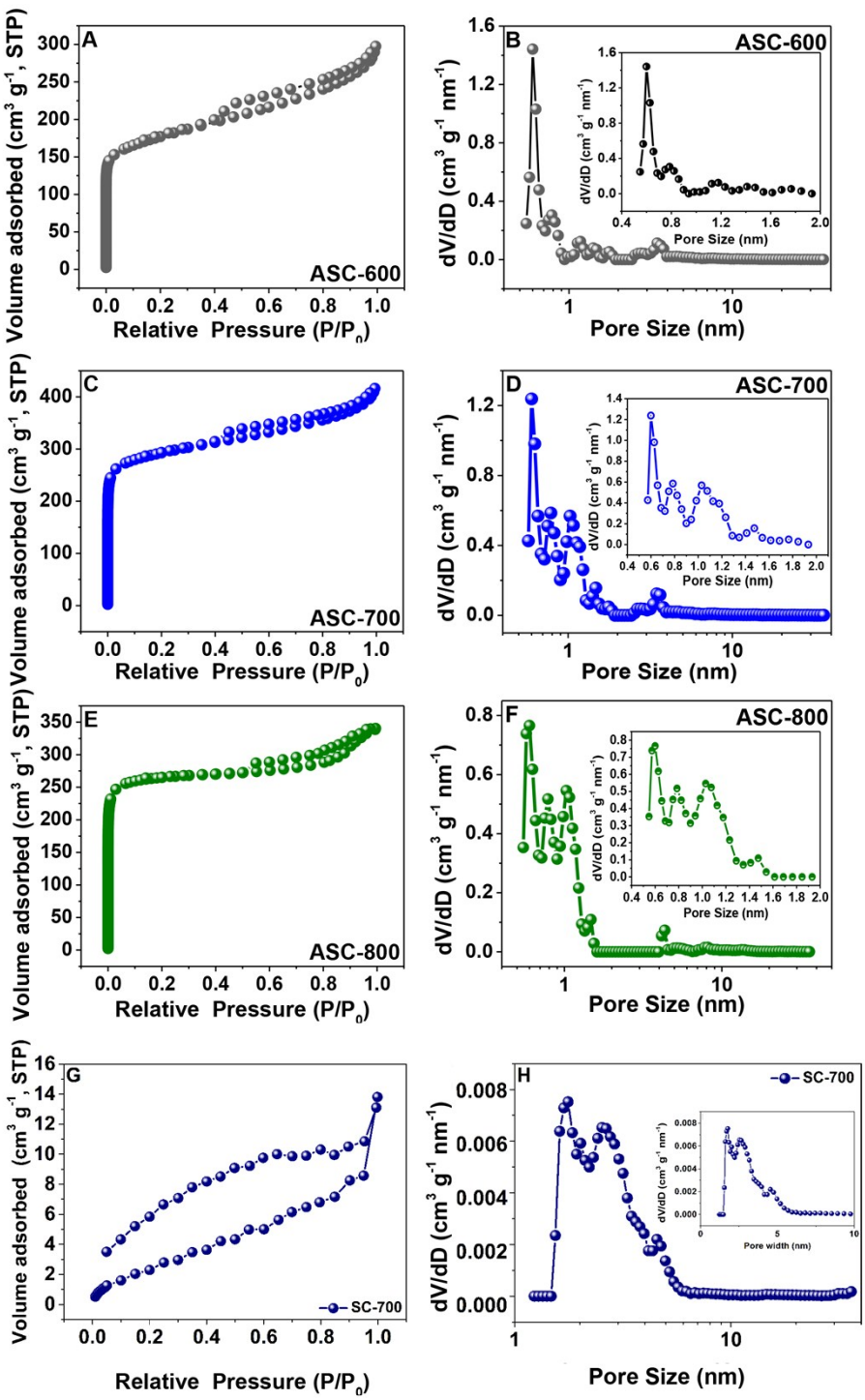


Fig. S4 (A, C, E and G) Nitrogen adsorption-desorption isotherms and (B, D, F and H) pore size distribution of ASC-Y and SC-700 calculated by DFT method.

Table S2 Porosity properties and specific capacitance of ASC-Y at current density of 1 A g⁻¹.

| Sample | S _{BET} ^a (m ² g ⁻¹) | S _{micro} ^b (m ² g ⁻¹) | V _{tot} ^c (cm ³ g ⁻¹) | V _{micro} ^d (cm ³ g ⁻¹) | Micropore size (nm) | Mesopore size (nm) | C _g ^e (F g ⁻¹) | C _s ^f (μF cm ⁻²) |
|---------|--|--|---|---|--------------------------------------|--|---|---|
| ASC-600 | 655.4 | 440.1 | 0.46 | 0.18 | 0.60, 0.79, 1.16, 1.43, 1.76 | 2.77, 3.49, 4.54, 4.97-6.53, 7.45, 10.71, 15.97, 22.95 | 330 | 50.4 |
| ASC-700 | 1123.8 | 907.4 | 0.64 | 0.36 | 0.60, 0.78, 0.90-1.29, 1.47, 1.77 | 2.77, 3.51, 4.15, 4.75, 7.44, 10.72, 13.42, 16.73, 23.5 | 401 | 35.7 |
| ASC-800 | 1060.5 | 1006.0 | 0.53 | 0.38 | 0.59, 0.79, 1.04, 1.47 13.58 | 4.31, 4.75-6.51, 8.05, 10.68, | 353 | 33.3 |
| SC-700 | 10.2 | - | 0.021 | - | - | 1.76, 2.53, 4.55 | 23.5 | - |

^a) BET Surface Area, ^b) t-Method micropore surface area, ^c) Total pore volume for pores with Diameter less than 332.41 nm at P/Po = 0.994240,

^d) DFT-Method micropore volume, ^e) Mass specific capacitance, ^f) Area specific capacitance.

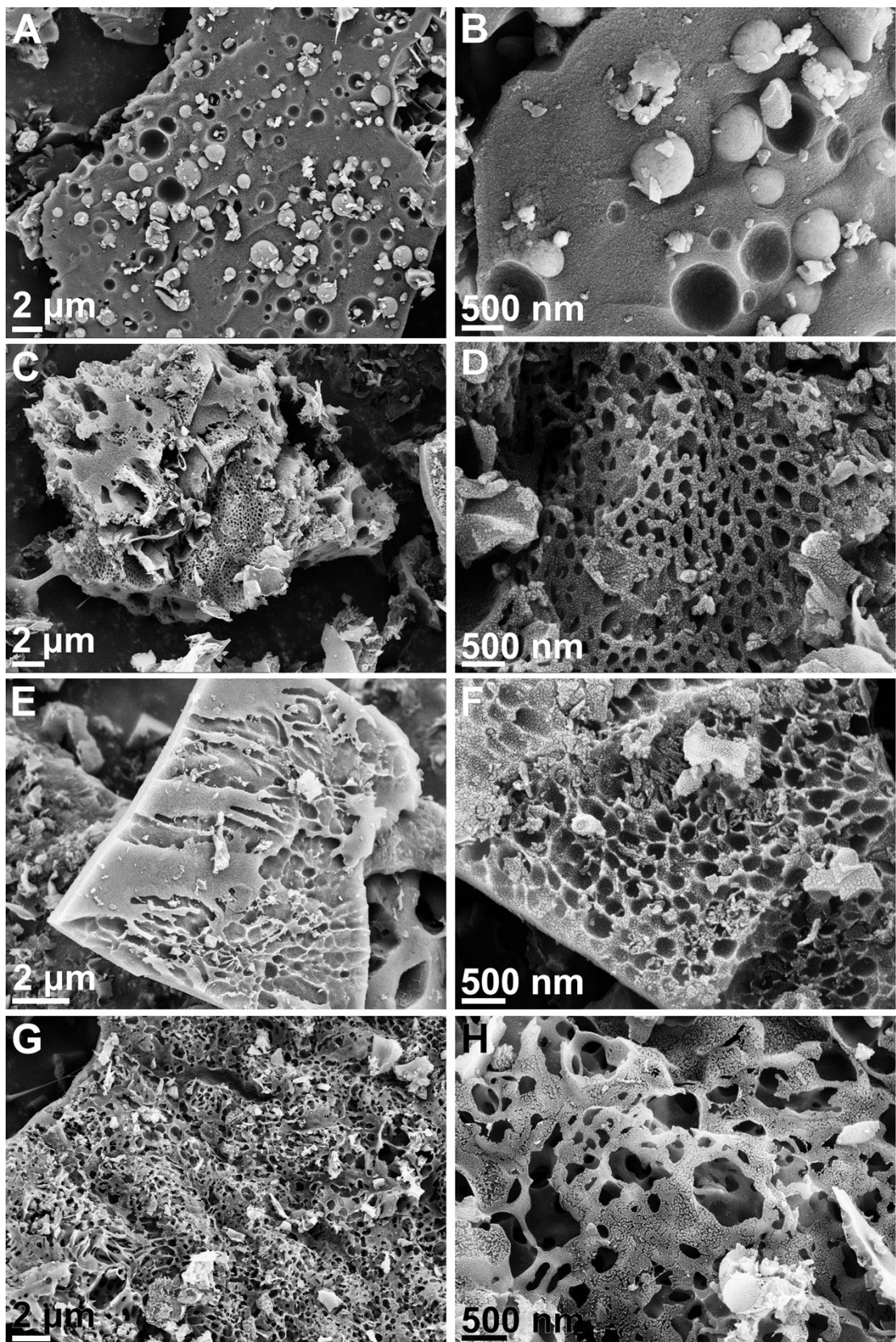


Fig. S5 SEM images of (A, B) SC-700; (C, D) ASC-600; (E, F) ASC-700; and (G, H) ASC-800.

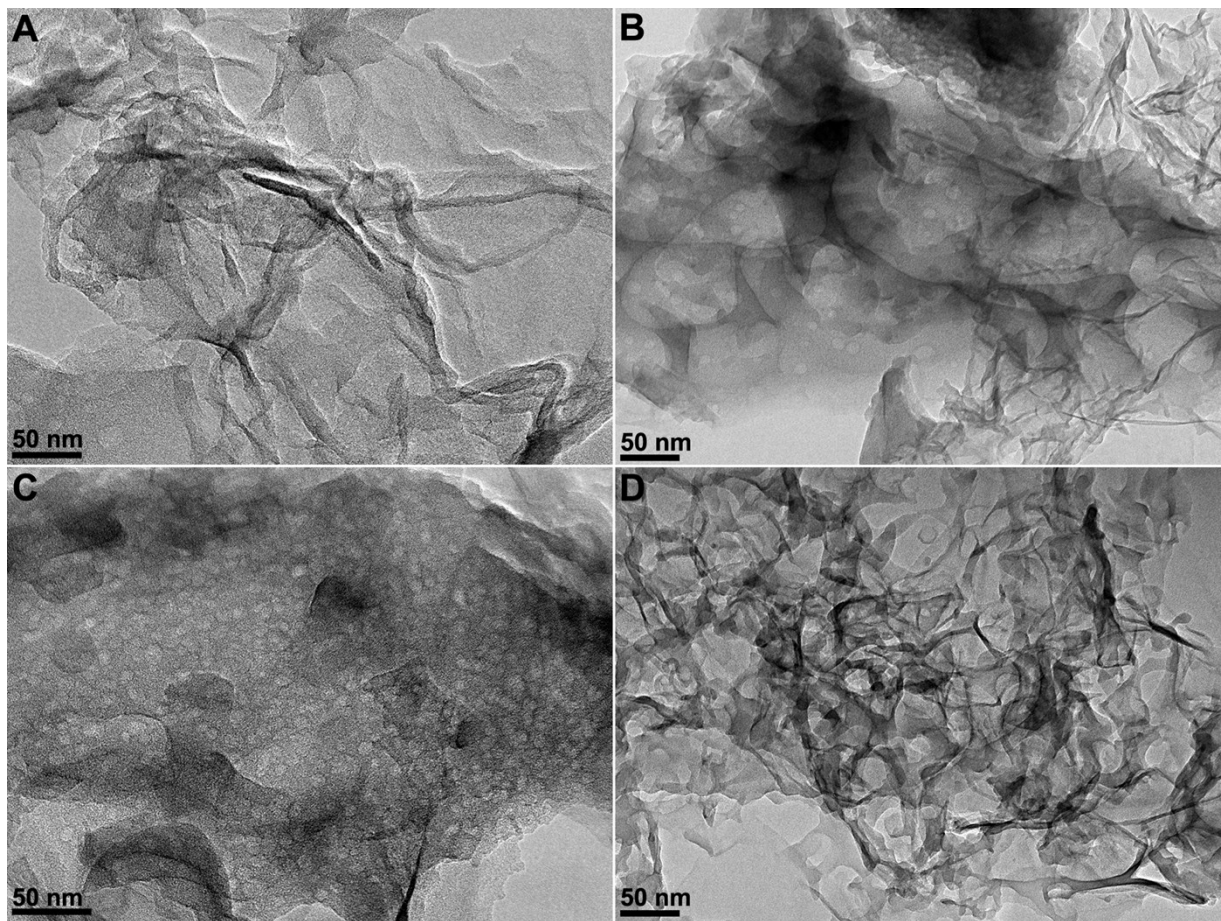


Fig. S6 TEM images of (A) SC-700, (B) ASC-600, (C) ASC-700, and (D) ASC-800.

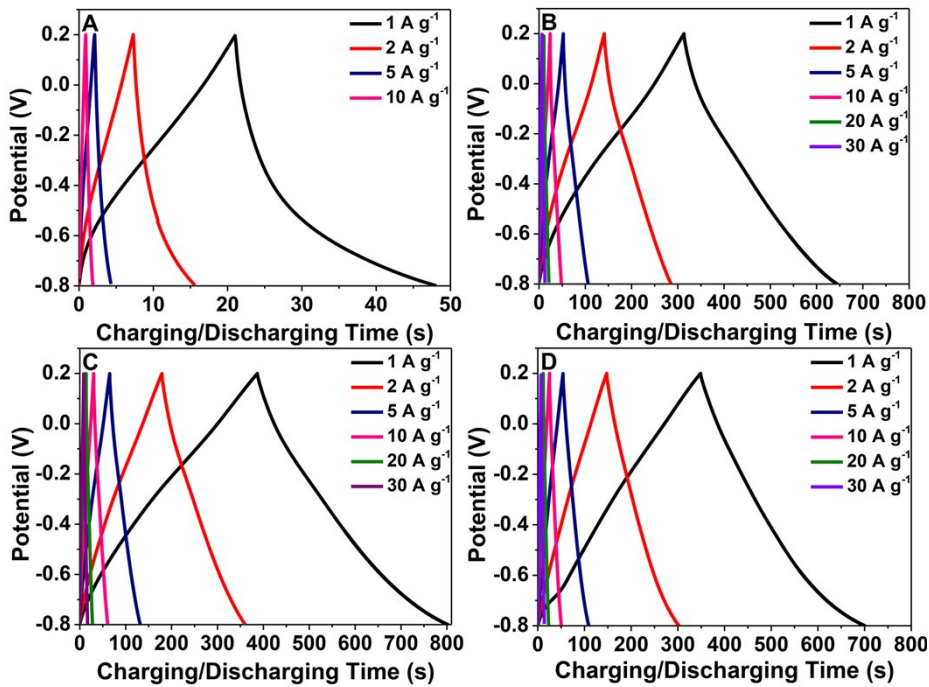


Fig. S7 GCD curves of (A) SC-700, (B) ASC-600, (C) ASC-700, (D) ASC-800 (three-electrode system).

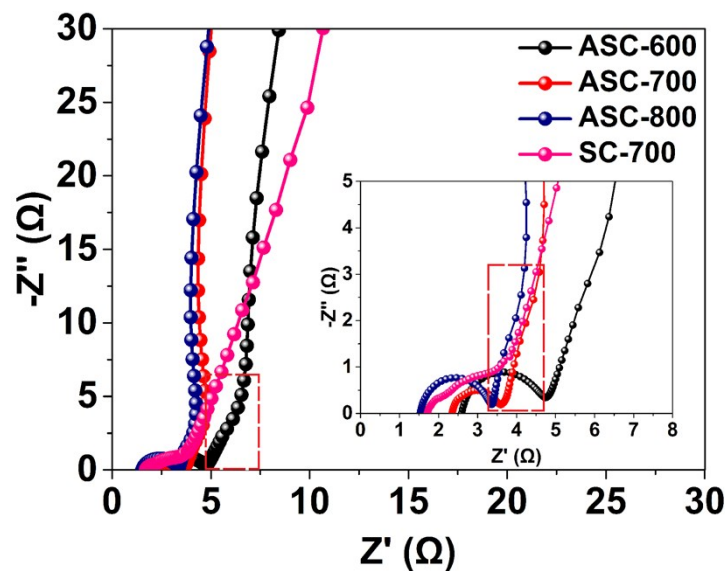


Fig. S8 Nyquist impedance plots of ASC-Y and SC-700 in at open circuit potential, where Y is 600, 700 and 800, respectively (three-electrode system).

As shown in Fig. S8, at the high- and medium-frequency region, after the semicircles are extended to intersect with the X-axis, the fitted radius of the semicircle is regarded as the internal resistance (R_{ct}) of the electrode.^{S1} It includes various resistive factors including electrical contact resistance between particles, ionic resistance of the electrolyte inside the porous structure, and charge transfer resistance.^{S2,S3} The evaluated values from EIS are 2.5, 1.3, 2.1, 3.3 Ω for ASC-600, ASC-700, ASC-800, and SC-700, respectively. These results confirm that a lower carbonization temperature generally renders a lower graphitization degree and a higher electrical resistance. It is known that activation agents can increase the content of surface oxygen species, and an excess of them, especially carboxyl group, has a negative impact on ion-transportation through inside the porous channels, and leads to high internal resistance.^{S1} Wide-micropores and small mesopores provide a high accessible surface area for ions absorption and desorption, leading to a low charge transfer resistance. Whereas interconnected mesopores and macropores facilitate rapid ion transport by supplying ion-buffering reservoirs and ion-transport pathways, meaning that the more the mesoporous and macropores, the smaller the ionic resistance inside the porous structure. Therefore, fewer ion accessible micropores and excessive carbonyl groups (e.g. SC-700, 3.3 Ω) will produce a high internal resistance, and fewer mesoporous and macropores could not serve enough channels for ion transportation, leading to ASC-800 (2.1 Ω) with a higher internal resistance (Table 1). Similarly, excessive carbonyl groups and a lower graphitization degree bring about a high internal resistance for ASC-600 (2.5 Ω). Therefore, carbon with a large accessible SSA and well matched PSD (that is, the size of the micropores suitable for the migration of electrolyte ions and a reasonable micropores / mesoporous or macropores ratio), will have good wettability, lower internal resistance (e.g. ASC-700, 1.3 Ω) and ideal capacitive characteristic (a vertical line at low-frequency region).^{S1}

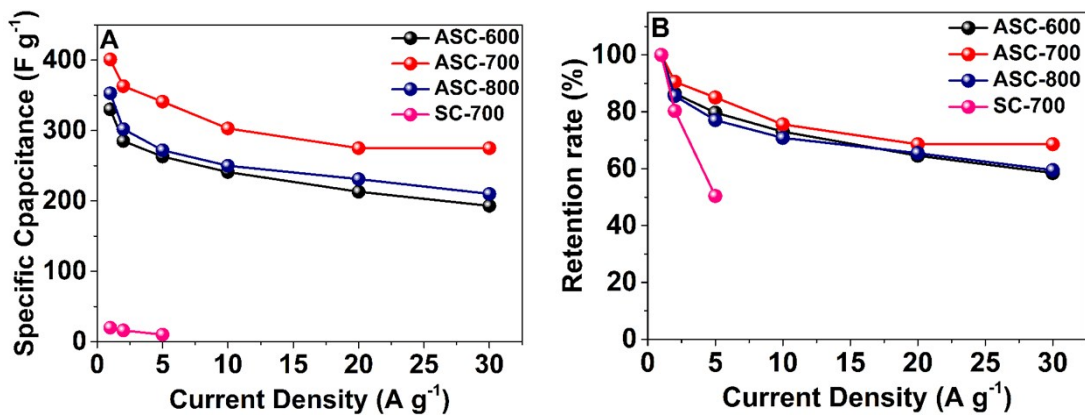


Fig. S9 (A) Specific capacitance (F g^{-1}) and (B) Retention rate (%) of three samples (ASC-Y) at different current densities in the three-electrode system.

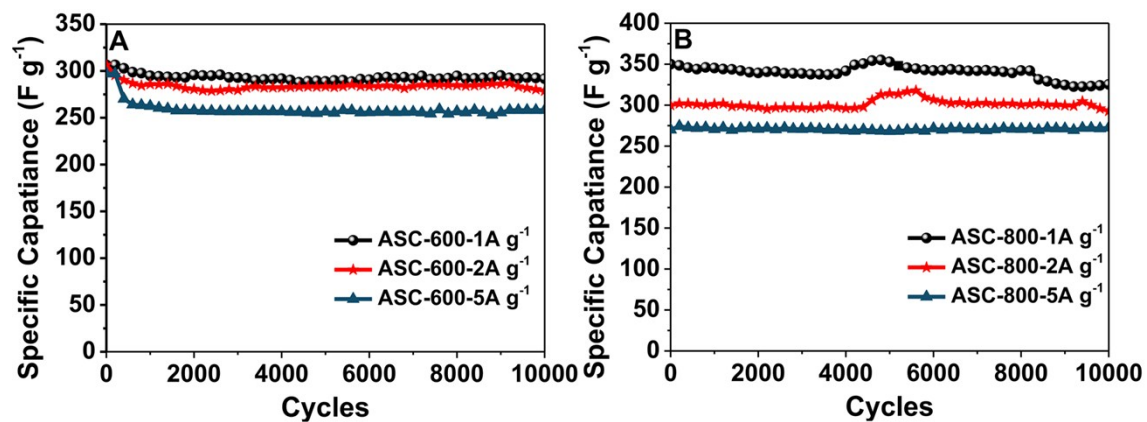


Fig. S10 Cycle stability of (A) ASC-600 and (B) ASC-800 at different current densities (three-electrode system).

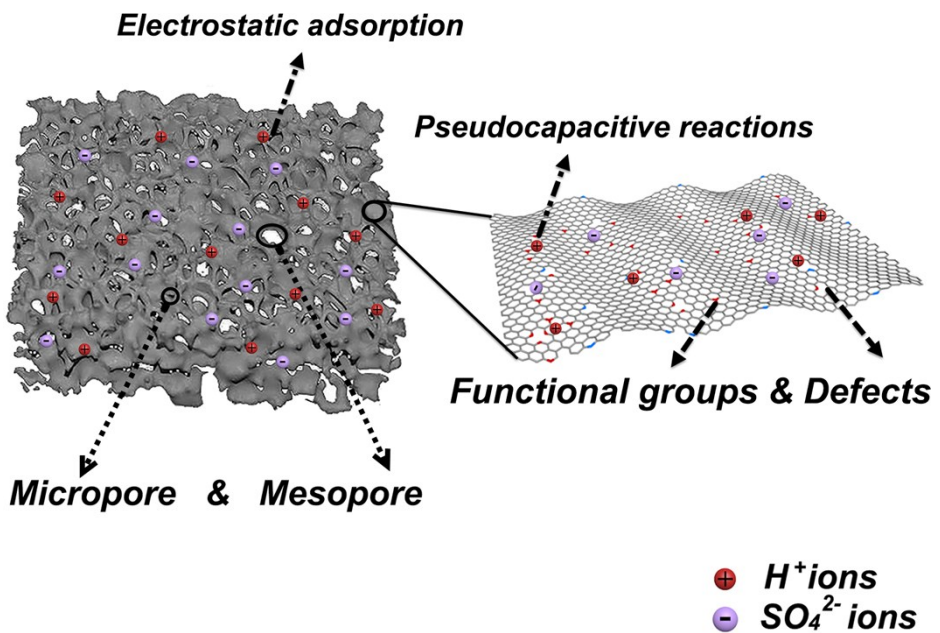


Fig. S11 Simulation of surficial status of sponge like porous carbons.

Activated semen cassiae (ASC) based carbon materials have hierarchical porous structures, which contain abundant micropores and mesopores. Such advantage means dual functions, including ions storage (micropores) and transport (mesopores). Moreover, functional groups and defects generated by heteroatoms and activation process will contribute to pseudocapacitance greatly. ^{S4}

Table S3 Specific gravimetric capacitances and cycle stability of ASC-700 in comparison with the biomass derived porous carbon materials in literatures (three-electrode system, aqueous solution as electrolyte).

| Precursor | Activation agents | C _g , Current density | Retention rate (%), Cycle numbers, | Literature |
|----------------------|---|---|--|------------------|
| Semen Cassiae | K₂C₂O₄·H₂O | 401 F g⁻¹, 1 A g⁻¹ | 88.1%, 10000, 1 A g⁻¹ | This work |
| | | 363 F g⁻¹, 2 A g⁻¹ | 90.3%, 10000, 2 A g⁻¹ | |
| | | 341 F g⁻¹, 5 A g⁻¹ | 94.5 %, 10000, 5 A g⁻¹ | |
| Perilla Frutescens | / | 270 F g ⁻¹ , 0.5 A g ⁻¹ | -- | Ref. S5 |
| Wild Jujube | KOH | 398 F g ⁻¹ , 0.5 A g ⁻¹ | 97 %, 10000, 5 A g ⁻¹ | Ref. S6 |
| Auricularia | KOH | 374 F g ⁻¹ , 0.5 A g ⁻¹ | 96 %, 10000, 200 mV s ⁻¹ | Ref. S7 |
| Bagasse Wastes | KOH | 320 F g ⁻¹ , 0.5 A g ⁻¹ | 92.85 %, 15000, 10 A g ⁻¹ | Ref. S8 |
| Cotton Fabric | KOH | 180 F g ⁻¹ , 0.5 A g ⁻¹ | 95 %, 10000 | Ref. S9 |
| Lotus Stems | / | 174 F g ⁻¹ , 5 mV s ⁻¹ | 72 %, 10000, 500 mV s ⁻¹ | Ref. S10 |
| Rice Straw | / | 332 F g ⁻¹ , 0.5 A g ⁻¹ | 99%, 10000, 10 A g ⁻¹ | Ref. S11 |
| Eucalyptus Leaves | KHCO ₃ | 372 F g ⁻¹ , 0.5 A g ⁻¹ | 97.5%, 15000, 10 A g ⁻¹ | Ref. S12 |
| Moringa Oleifera | KOH | 374 F g ⁻¹ , 0.5 A g ⁻¹ | 95%, 20000, 20 A g ⁻¹ | Ref. S13 |

| | | | | |
|-------------------------------|--|---|--|------------|
| Honey | KOH | 271 F g^{-1} , 1 A g^{-1} | 98% , 3000 , 10 A g^{-1} | Ref. S14 |
| Precursor | Activation agents | C_g , Current density | Retention rate (%), Cycle numbers, | Literature |
| Nori | ZnCl_2 | 220 F g^{-1} , 0.1 A g^{-1} | 96.6% , 5000 , 2 A g^{-1} | Ref. S15 |
| Pteroceltis Tatarinowii Maxim | ZnCl_2 | 206 F g^{-1} , 0.5 A g^{-1} | 99% , 10000 , 3 A g^{-1} | Ref. S16 |
| Wheat Straw | $49\% \text{ ZnCl}_2 + 51\% \text{ KCl}$ | 223.9 F g^{-1} , 0.5 A g^{-1} | 91.4% , 10000 , 50 mV s^{-1} | Ref. S17 |
| Mycelium Pellets | ZnCl_2 | 219.4 F g^{-1} , 1 A g^{-1} | 99.6% , 5000 , 20 mV s^{-1} | Ref. S18 |
| Lignocellulose | $\text{ZnCl}_2\text{-NaH}_2\text{PO}_4$ | 193.6 F g^{-1} , 1 A g^{-1} | 97.9% , 10000 , 100 mV s^{-1} | Ref. S19 |

References

- [S1] J. -S. Wei, H. Ding, Y. -G. Wang and H. -M. Xiong, *ACS Appl. Mater. Interfaces*, 2015, **7**, 5811-5819.
- [S2] C. Yang, C. -Y. V. Li, F. Li, and K. -Y Chan, *J. Electrochem. Soc.*, 2013, **160**, H271-H278.
- [S3] Y. Mun, C. Jo, T. Hyeon, J. Lee, K. -S. Ha, K. -W. Jun, S. -H. Lee, S. -W Hong, H. I. Lee, S. Yoon, and J. Lee, *Carbon*, 2013, **64**, 391-402.
- [S4] M. -X. Liu, L. -Y. Chen, D. -Z. Zhang, H. Duan, W. Xiong, Z.-J. Xu, L. -H. Gan and L.-W. Chen, *Chin. Chem. Lett.*, 2016, **27**, 299-404.
- [S5] B. Liu, Y. Liu, H. Chen, M. Yang and H. Li, *J. Power Sources*, 2017, **341** 309-317.
- [S6] K. Sun, S. Yu, Z. Hu, Z. Li, G. Lei, Q. Xiao and Y. Ding, *Electrochim. Acta*, 2017, **231**, 417-428.
- [S7] C. Long, X. Chen, L. Jiang, L. Zhi and Z. Fan, *Nano Energy*, 2015, **12**, 141-151.
- [S8] H. Feng, H. Hu, H. Dong, Y. Xiao, Y. Cai, B. Lei, Y. Liu and M. Zheng, *J. Power Sources*, 2016, **302**, 164-173.
- [S9] L. Chen, T. Ji, L. Mu and J. Zhu, *Carbon*, 2017, **111**, 839-848.
- [S10] Y. Zhang, S. Liu, X. Zheng, X. Wang, Y. Xu, H. Tang, F. Kang, Q.-H. Yang and J. Luo, *Adv. Funct. Mater.*, 2017, **27**, 1604687.
- [S11] N. Sudhan, K. Subramani, M. Karnan, N. Ilayaraja and M. Sathish, *Energy & Fuels*, 2017, **31**, 977-985.
- [S12] A. K. Mondal, K. Kretschmer, Y. Zhao, H. Liu, C. Wang, B. Sun and G. Wang, *Chem. - Eur. J.*, 2017, **23**, 3683-3690.
- [S13] Y. Cai, Y. Luo, Y. Xiao, X. Zhao, Y. Liang, H. Hu, H. Dong, L. Sun, Y. Liu and M. Zheng, *ACS Appl Mater Interfaces*, 2016, **8**, 33060-33071.
- [S14] J. Li, G. Zan, Q. Wu, *New J. Chem.*, 2015, **39**, 8165-8171.
- [S15] C. Wang and T. Liu, *J. Alloy Compd.*, 2017, **696**, 42-50.
- [S16] Z. Sun, J. Liao, B. Sun, M. He, X. Pan, J. Zhu, C. Shi and Y. Jiang, *Int. J. Electrochem. Sci.*, 2017, **12**, 12084-12097.

- [S17] S. Zhang, K. Tian, B. -H. Cheng and H. Jiang, *ACS Sustainable Chem. Eng.* 2017, **5**, 6682-6691.
- [S18] J. Hao, Y. Huang, C. He, W. Xu, L. Yuan, D. Shu, X. Song and T. Meng, *Sci. Rep.*, 2018, **8**, 562-560.
- [S19] J. Yi, Y. Qing, C. Wu, Y. Zeng, Y. Wu, X. Lu and Y. Tong, *J. Power Sources*, 2017, **351**, 130-137.